Phase fluctuations of linearly chirped solitons in a noisy optical fiber channel with varying dispersion, nonlinearity, and gain

Shihua Chen,[1,2] Y. H. Yang,[1] Lin Yi,[2] Peixiang Lu,[3] and Dong-Sheng Guo[3,4]
[1]*Department of Physics, Southeast University, Nanjing 210096, China*
[2]*Department of Physics, Huazhong University of Science and Technology, Wuhan 430074, China*
[3]*Wuhan National Laboratory for Optoelectronics, Wuhan 430074, China*
[4]*Department of Physics, Southern University, Baton Rouge, Louisiana 70813, USA*
(Received 28 October 2006; published 29 March 2007)

The phase fluctuations of arbitrarily nonlinearity- and dispersion-managed solitons propagating in a noisy fiber channel are studied both analytically and numerically. We begin by discussing the stability problem of such linearly chirped solitons with a full linear stability analysis. It is shown that these sophisticated solitons possess an enhanced stability against perturbations and therefore hold promise for applications in optical telecommunications. We then make an approach to the phase statistics of these solitons, which stems from an inevitable random walk in phase evolutions due to amplified spontaneous emission noise. By using the variational approach together with impulse-response (Green) functions, an elegant closed-form expression for the phase variance is derived based on an unconstrained self-similar soliton ansatz in which the effect of chirp fluctuations has been critically taken into account as well as the dispersive and nonlinear effects. An inspection of the intriguing subtleties of the interplay among these effects reveals that the chirp fluctuations effect does play an important role in the control of nonlinear phase noise via fiber dispersion, independently of whether the input solitons are initially chirped or not. Our analytical result also offers many possibilities of optimally manipulating nonlinear phase noise with engineered fiber parameters that may lead to the steady pulse propagation, broadening, or compression under favorable parametric conditions. Last, we demonstrate our result by several convincible examples and show an excellent agreement between analytical predictions and numerical simulations.

DOI: 10.1103/PhysRevE.75.036617 PACS number(s): 42.81.Dp, 42.65.Tg, 05.40.Fb, 05.10.Gg

I. INTRODUCTION

One of the most exciting highlights of optical soliton research is an establishment of the concept of dispersion management (DM) [1], which mainly arises from an impetus of the burgeoning demand for optical telecommunications. This unique concept manifests itself by allowing for a propagation of robust solitary waves in the system with a periodic concatenation of fiber segments or even very different elements [2]. For this reason, the solitary waves involved are thereafter called DM solitons to make them distinct from ordinary solitons. As a consequence of a balance between nonlinearity and effective dispersion, DM solitons display many alluring properties such as enhanced peak power, higher dispersion tolerance, reduced timing jitter caused by amplifier noise [1,3], and being less deteriorated by four-wave mixing from soliton-soliton collisions [4]. In view of these promising advantages, it is not surprising that to date, almost all experiment demonstrations or field trials of ultra-high-speed long-haul optical soliton transmissions are performed exclusively with such DM soliton formats [5].

Additionally, more and more effort has been devoted to the study of soliton propagations with nonlinearity management, an analog of DM concept [6–10]. Numerical evidences show that nonlinearity management, always combined with DM when designing communication lines, can offer effective ways of increasing the bit rates [6], suppressing the spectral sidebands [7], and reducing the nonlinear phase noise [8]. It is a good candidate for establishing the best trade-off between low-cost requirements and the high optical signal-to-noise ratio [9]. Although the experimental realization reported in Ref. [10] is very trivial, the management of nonlinearity that alternates in sign is also possible in implementation, relying on the presence of appropriate materials such as periodically poled lithium niobate waveguides [11] and self-defocusing semiconductors [12]. Moreover, new possibilities that the nonlinearity and dispersion are simultaneously managed can be made decidedly real in the future through gas-filled photonic crystal fibers because of their greatly enhanced design freedom and feasible nonlinearity control [13].

Further than that, the dynamics of nonlinearity- and dispersion-managed solitons, or linearly chirped solitons, has been explored theoretically by the use of an extended inverse scattering transform method [14] and some symmetry reduction techniques [15–18]. The underlying model frequently exploited is the generalized nonlinear Schrödinger (NLS) equation with varying coefficients, i.e., allowing dispersion, nonlinearity, and gain profiles to change with the propagation distance. In its own right, this model admits of parabolic similaritons and linearly chirped solitons under different favorable conditions [19], both of which possess such universal features as a self-similarity in pulse shape and an enhanced linearity in pulse chirp [14–20]. In view of the well-known fact that the self-similarity stabilizes similaritons [20], a natural question arises as to whether the same applies to these linearly chirped solitons. Although numerical simulations performed previously give a positive answer to this question [14–17], an affirmative answer requires a full linear stability analysis of these solitons, which will be presented in this paper for the first time.

 ©2007 The American Physical Society

Also of primary concern is the random walk in phase evolutions for such linearly chirped solitons propagating in a noisy optical fiber channel, an issue closely related to the optical differential-phase-shift keying transmissions in which information is encoded in the phase difference between successive symbols [21]. Using the variational approach [22,23] along with impulse-response functions, we present here an exact closed-form expression for their phase variance, in consideration of the combined effects of dispersion [24], nonlinearity [25], and chirp fluctuations [26]. It is clearly seen that either the dispersion effect or the chirp fluctuations effect does play an important role in producing nonlinear phase noise as well as the one due to nonlinearity (often called the Gordon-Mollenauer effect [25]). In terms of this expression, one can gain insight into the subtle effect that may contribute or mitigate the nonlinear phase noise for each of the initial or fiber parameters involved, and thereby can find a possible route to the optimization of parameters for phase-modulated soliton communications. We corroborate this analytical result by direct numerical simulations via several typical examples. It is shown that the nonlinear phase noise can be well manipulated, including either significantly reduced or sharply enhanced, by using appropriate profiles of dispersion and nonlinearity. Meanwhile, we also show that the effects of input soliton parameters such as pulse width, frequency shift, and chirp parameter are non-negligible in the control of total phase noise. In particular, the impact of initial frequency shift on phase noise is demonstrated to be decidedly detrimental throughout.

The paper is organized as follows. Section II reviews the generalized NLS equation with varying coefficients and provides its bright soliton solutions under a certain parametric condition. In order to capture the role of self-similarity in stabilizing these sophisticated solitons, a full linear stability analysis is performed in Sec. III. As solitons propagate in a noisy optical fiber channel, their phase evolutions will undergo random walks due to amplified spontaneous emission (ASE) noise. We then calculate their phase variance analytically using the variational approach together with impulse-response functions in Sec. IV. Also included there is an analytical derivation of the variance of chirp jitter. In terms of the closed-form expression for phase variance, we present a detailed discussion on soliton phase statistics in Sec. V. Typically, three intriguing cases are discussed there to demonstrate our analytical predictions as compared with numerical simulations. Finally, Sec. VI concludes the paper.

II. SELF-SIMILAR SOLITON SOLUTIONS

As is well known, the problem of soliton management in the picosecond regime can be described by the generalized NLS equation with varying coefficients [14–19],

$$i\psi_z = \frac{\beta(z)}{2}\psi_{\tau\tau} - \gamma(z)|\psi|^2\psi + i\frac{g(z)}{2}\psi, \tag{1}$$

where $\psi(z,\tau)$ is the complex envelope of the electric field in a comoving frame, z is the propagation distance, τ is the retarded time, $\beta(z)$ is the group-velocity dispersion parameter, $\gamma(z)$ is the nonlinearity parameter, and $g(z)$ is the distributed gain function. The subscripts z and τ denote the spatial and temporal partial derivatives. We note that this equation was intensively explored in the past and various types of self-similar solutions were obtained under different favorable conditions. Here we only outline the exact self-similar soliton solutions [19]

$$\psi_s(z,\tau) = \sqrt{\frac{E(z)}{2T(z)}}F(\theta)\exp[i\vartheta(z,\tau)], \tag{2}$$

where $E(z)=E_0\exp[\int_0^z g(z')dz'] \equiv E_s(z)$ denotes the soliton energy, $T(z)=\tau_0[1-2c_0D(z)] \equiv T_s(z)$ accounts for the pulse width, $D(z)=\int_0^z \beta(z')dz'$ is the accumulated dispersion, $F(\theta)=\mathrm{sech}(\theta)$ is a real function with the self-similar variable $\theta(z,\tau)=[\tau-\tau_p(z)]/T(z)$, the pulse position is given by $\tau_p(z)=\tau_c-b_0D(z)\equiv\tau_{ps}(z)$, and the phase $\vartheta(z,\tau)$ takes the quadratic form

$$\vartheta(z,\tau) = \phi(z) + b(z)[\tau-\tau_p(z)] + c(z)[\tau-\tau_p(z)]^2, \tag{3}$$

with the following z-dependent coefficients:

$$\phi(z) = \phi_0 - \frac{1}{2\tau_0}\frac{D(z)}{T_s(z)} - \frac{b_0^2}{2}D(z) \equiv \phi_s(z),$$

$$b(z) = b_0 \equiv b_s(z), \quad \text{and} \quad c(z) = \frac{c_0\tau_0}{T_s(z)} \equiv c_s(z).$$

Here the parameters E_0, ϕ_0, b_0, c_0, τ_0, and τ_c are integration constants representing the initial values of pulse energy, phase offset, frequency shift, chirp, width, and central position, respectively. The parameters with subscript s stand for the deterministic soliton characteristics without the presence of noise, aiming to distinguish them from those obtained under noise.

We emphasize that such self-similar solutions form only under the parametric condition

$$g(z) = 2c_s(z)\beta(z) + \rho(z)^{-1}\frac{d}{dz}\rho(z), \tag{4}$$

where $\rho(z)\equiv\beta(z)/\gamma(z)(<0)$ and $c_s(z)$ is defined above. Most recently, a self-similar soliton propagation under this condition has been experimentally observed in a comblike decreasing-dispersion fiber amplifier [27]. It is apparent that the fiber parameters required for soliton formation cannot be chosen independently, and that different signs of input chirp parameter c_0 correspond to different fiber gain (or loss) for given fiber dispersion and nonlinearity. If $c_0=0$, it easily follows that a chirp-free DM soliton may survive an appropriate gain profile. In addition, one can conclude from Eqs. (2)–(4) that the evolutions of pulse width, pulse position, phase offset, and chirp parameter are uniquely determined by the accumulated dispersion, irrespective of the profiles of local dispersion and nonlinearity, which only affect the soliton energy or peak power through the ratio $\rho(z)$.

It is well known that the self-similarity can stabilize optical similaritons against optical wave breaking [20], but now a natural question arises: Are these self-similar solutions stable and which role does the self-similarity play in stabi-

lizing them? The answer to the former question is obviously definite because these self-similar solutions are confirmed as genuine solitons by Serkin *et al.* [14,28]. This is also the main reason for us to call the solution (2) the self-similar solitons since the self-similarity in itself does not contradict the soliton concept [29]. As for the latter question, only a positive answer was presented in the past with numerical simulations [14–17]. In the ensuing section, we will perform a full linear stability analysis of such self-similar solutions and wish to provide an affirmative answer to both questions.

III. LINEAR STABILITY ANALYSIS

To analyze the stability of self-similar solutions (2) with respect to small perturbations, we linearize Eq. (1) on the soliton background

$$\psi(z,\tau) = \sqrt{\frac{E(z)}{2T(z)}}\left\{F(\theta) + f(\theta)\exp\left[-i\lambda\frac{D(z)}{\tau_0 T(z)}\right] + h^*(\theta)\exp\left[i\lambda^*\frac{D(z)}{\tau_0 T(z)}\right]\right\}\exp[i\vartheta(z,\tau)], \tag{5}$$

where $f(\theta)$ and $h(\theta)$ are complex, small perturbation functions, λ is a complex number, and the asterisk stands for the complex conjugation [30]. After ignoring the nonlinear terms for $f(\theta)$ and $h(\theta)$, we obtain the linear eigenvalue problem, which can be written in the matrix form

$$\mathbf{L}\Psi = \lambda\Psi, \tag{6}$$

where $\Psi=(f,h)^{\mathrm{T}}$ and

$$\mathbf{L} = \begin{pmatrix} \frac{1}{2}\frac{d^2}{d\theta^2} - \frac{1}{2} + 2F^2 & F^2 \\ -F^2 & -\frac{1}{2}\frac{d^2}{d\theta^2} + \frac{1}{2} - 2F^2 \end{pmatrix}, \tag{7}$$

where the superscript T denotes a matrix transposition.

We note that the linear operator $\mathbf{L}$ is self-adjoint, and therefore its eigenfunctions are also self-adjoint with real eigenvalues λ [31]. Since this operator has the same form as the one for the famous integrable cubic NLS equation with constant coefficients [32], we can find easily its complete eigenfunctions and eigenvalues. We begin with its continuous-wave functions and continuums

$$\Psi_c = \frac{\exp(-ik\theta)}{(k+i)^2}\left\{[k^2 - 1 - 2ik\tanh(\theta)]\begin{pmatrix}1\\0\end{pmatrix} + \mathrm{sech}^2(\theta)\begin{pmatrix}1\\1\end{pmatrix}\right\}, \quad \lambda_\Psi = -\frac{1}{2}(k^2+1), \tag{8}$$

$$\bar{\Psi}_c = \sigma_1\Psi_c, \quad \lambda_{\bar{\Psi}} = \frac{1}{2}(k^2+1), \tag{9}$$

where σ_1 is a Pauli spin matrix and k is an arbitrary real parameter. Besides, the bound states for $\mathbf{L}$, often called neutral modes, also can be found by searching for discrete eigenvalues. Obviously, for $\lambda=0$, we can obtain the following neutral modes:

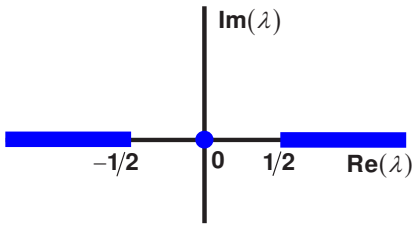

FIG. 1. (Color online) Schematic structure of the spectra of the linear eigenvalue problem (6) with the shaded regimes corresponding to the discrete "0" and continuums $|\lambda|>1/2$.

$$\Psi_e = F(\theta)\begin{pmatrix}1\\-1\end{pmatrix}, \quad \Psi_o = \frac{d}{d\theta}F(\theta)\begin{pmatrix}1\\1\end{pmatrix}, \tag{10}$$

which correspond to the gauge transform and infinitesimal self-similar translation of the solution $F(\theta)$. Any linear combination of these neutral modes can constitute the bound-state solutions to Eq. (6). One can verify that for such systems, there do not exist other discrete eigenvalues in the gap of continuums, i.e., $|\lambda|<1/2$ [33]. Nevertheless, it is necessary to introduce another two associated discrete-spectrum modes Ψ_1 and Ψ_2 for closure, which satisfy inhomogeneous equations [32,33]

$$\mathbf{L}\Psi_1 = \Psi_o, \quad \mathbf{L}\Psi_2 = \Psi_e. \tag{11}$$

After a little algebra, we write them in an explicit form

$$\Psi_1 = \theta F(\theta)\begin{pmatrix}1\\-1\end{pmatrix}, \quad \Psi_2 = \frac{1-\theta\tanh(\theta)}{\cosh(\theta)}\begin{pmatrix}1\\1\end{pmatrix}. \tag{12}$$

As a result, the system of functions given by Eqs. (8)–(10) and (12) forms a complete space and thus does not admit other localized modes in it.

As is evident from Eq. (5), the soliton dynamics may display the linear instability if the eigenvalue λ is imaginary, or the periodic long-term oscillations if λ is real. Since here all eigenvalues, including continuums and the discrete "0," are real (see Fig. 1), the soliton solutions (2) are unconditionally stable, which clearly provides an elegant answer to the first question on an analytical level. Particularly, we find from Eq. (5) that even if the eigenvalue were imaginary, for instance, an imaginary λ would occur as the model (1) is perturbed by the nonlinear gain [17], the dynamics of solitons or solitary waves also can be stabilized by managing the dispersion map such that the accumulated dispersion $D(z)$ is small enough on an average. Due to the fact that Eq. (5) is a direct consequence of the self-similarity imposed on Eq. (2), we may argue that the self-similarity really plays an enhanced role in stabilizing the solitons for an appropriate dispersion map, just as indicated by numerical simulations in Ref. [17]. Therefore, an affirmative answer to the second question is obtained immediately as well.

IV. RANDOM PHASE FLUCTUATIONS

Although the self-similar solitons may exhibit an enhanced stability in pulse shape, they also suffer from a random walk in their phase evolutions when propagating in a

noisy optical fiber channel. In this section, we will present an analytical calculation of the phase jitter for such solitons. For our studies, a complex stochastic term $\hat{\Gamma}(z,\tau)$ has been explicitly added in Eq. (1), viz.,

$$i\psi_z = \frac{\beta(z)}{2}\psi_{\tau\tau} - \gamma(z)|\psi|^2\psi + i\frac{g(z)}{2}\psi + \hat{\Gamma}(z,\tau). \tag{13}$$

For simplicity, this stochastic noise term is assumed to possess the zero mean and the correlation

$$\langle \hat{\Gamma}(z,\tau)\hat{\Gamma}^*(z',\tau')\rangle = 2\Gamma_0\delta(z-z')\delta(\tau-\tau'), \tag{14}$$

where $\langle\ \rangle$ stands for an ensemble average and Γ_0 is the white noise intensity. The practical relevance to such a noise is the ASE noise imposed by optical amplifiers which has an additive nature [34]. Obviously, in the absence of this noise term, a deterministic soliton behavior can be described by Eq. (2) with the parametric condition (4). But, such a deterministic behavior usually becomes stochastically complicated when adding the noise (14), and therefore an analysis of it frequently needs to resort to numerical simulations. Fortunately, the dynamics of soliton parameters can still be well understood by using the variational approach [22,23], the moment method [35,36], and the soliton perturbation theory [32,37] when the noise perturbations are small. All these analytical tools are satisfactory to a large extent for applications in diverse areas, and their advantages and/or disadvantages are extensively discussed over the years [37,38].

A. Variational approach

In this work, we will employ the variational approach to investigate the dynamics of soliton parameters in a systematical manner (noting that the moment-method description of the same problem, although somewhat conceptually simpler, needs more algebraic skills and has been dealt with elegantly in our subsequent work, showing good consistency with the variational description here [39]). Since there exists no direct Lagrangian for it, Eq. (13) must be transformed into an appropriate form. By setting $\psi(z,\tau)=\sqrt{\mathcal{I}(z)}\varphi(z,\tau)$, where $\mathcal{I}(z)=\exp[\int_0^z g(z')dz']$, we can rewrite it as

$$i\varphi_z = \frac{\beta(z)}{2}\varphi_{\tau\tau} - \gamma(z)\mathcal{I}(z)|\varphi|^2\varphi + \frac{1}{\sqrt{\mathcal{I}(z)}}\hat{\Gamma}(z,\tau). \tag{15}$$

This equation can be readily reproduced via the Euler-Lagrange equation if one posits the Lagrangian density

$$\mathcal{L}(z,\tau) = \frac{i}{2}(\varphi^*\varphi_z - \varphi\varphi_z^*) + \frac{1}{2}(\beta|\varphi_\tau|^2 + \gamma\mathcal{I}|\varphi|^4) - \frac{1}{\sqrt{\mathcal{I}}}(\hat{\Gamma}\varphi^* + \hat{\Gamma}^*\varphi). \tag{16}$$

Integrating both sides of Eq. (16) over time, we obtain the average Lagrangian

$$L(z) = \frac{1}{\mathcal{I}}\int_{-\infty}^{\infty}\left[\frac{1}{2}(\beta|\psi_\tau|^2 + \gamma|\psi|^4) - \mathrm{Im}(\psi^*\psi_z)\right]d\tau - \frac{2}{\mathcal{I}}\int_{-\infty}^{\infty}\mathrm{Re}(\hat{\Gamma}\psi^*)d\tau, \tag{17}$$

and the reduced Euler-Lagrange equation

$$\frac{d}{dz}\left(\frac{\partial L}{\partial \mathbb{S}_z}\right) - \frac{\partial L}{\partial \mathbb{S}} = 0, \tag{18}$$

where $\mathbb{S}$ denotes the pulse characteristics only related to the distance z. By means of Eq. (18), the dynamic equations for soliton parameters can be obtained with an appropriate sech-shaped or Gaussian pulse ansatz.

Here, according to the proposals by McKinstrie *et al.* [23], we employ an unconstrained soliton ansatz (2), in which the pulse energy $E(z)$, width $T(z)$, pulse position $\tau_p(z)$, phase offset $\phi(z)$, frequency $b(z)$, and chirp parameter $c(z)$ are all now assumed to be random independent quantities. Accordingly, by using the Stratonovich prescription, one can obtain from Eq. (18) a system of Langevin equations with multiplicative noise

$$\frac{dE}{dz} = gE + \mathrm{Re}\int_{-\infty}^{\infty} g_E^*(z,\tau)\hat{\Gamma}d\tau, \tag{19}$$

$$\frac{dT}{dz} = -2\beta cT + \mathrm{Re}\int_{-\infty}^{\infty} g_T^*(z,\tau)\hat{\Gamma}d\tau, \tag{20}$$

$$\frac{dc}{dz} = 2\beta c^2 - \frac{\gamma}{\pi^2T^3}\left(\frac{2\rho}{T} + E\right) + \mathrm{Re}\int_{-\infty}^{\infty} g_c^*(z,\tau)\hat{\Gamma}d\tau, \tag{21}$$

$$\frac{d\tau_p}{dz} = -\beta b + \mathrm{Re}\int_{-\infty}^{\infty} g_{\tau_p}^*(z,\tau)\hat{\Gamma}d\tau, \tag{22}$$

$$\frac{db}{dz} = \mathrm{Re}\int_{-\infty}^{\infty} g_b^*(z,\tau)\hat{\Gamma}d\tau, \tag{23}$$

$$\frac{d\phi}{dz} = -\frac{\beta}{2}b^2 + \frac{\beta}{3T^2} + \frac{5\gamma E}{12T} + \mathrm{Re}\int_{-\infty}^{\infty} g_\phi^*(z,\tau)\hat{\Gamma}d\tau, \tag{24}$$

where Re stands for the real part of the integrals and the projection functions within the integrals are given by

$$g_E(z,\tau) = 2i\psi_s, \tag{25}$$

$$g_T(z,\tau) = i\frac{T}{E}\left(\frac{12}{\pi^2}\theta^2 - 1\right)\psi_s, \tag{26}$$

$$g_c(z,\tau) = \frac{6}{\pi^2ET^2}[1 - 2\theta\tanh(\theta)]\psi_s, \tag{27}$$

$$g_{\tau_p}(z,\tau) = i\frac{2T}{E}\theta\psi_s, \tag{28}$$

$$g_b(z,\tau) = \frac{2}{E}\left[i2cT\theta - \frac{1}{T}\tanh(\theta) \right]\psi_s, \tag{29}$$

$$g_\phi(z,\tau) = \frac{1}{E}\left[i2bT\theta - \frac{3}{2} + \theta\tanh(\theta) \right]\psi_s. \tag{30}$$

We note that in the absence of noise, these dynamic equations yield the identical soliton entities given by Eqs. (2) and (3) with deterministic soliton parameters E_s, T_s, τ_{ps}, ϕ_s, b_s, and c_s. But in their present forms, they govern the statistics of the soliton parameters under the ASE noise. Here the reason for us to choose the Stratonovich prescription, not an Ito one, lies in the fact that the ordinary chain rule for soliton variational theory does apply to Stratonovich calculus, but fails in Ito calculus [40].

In addition, we note that, in a first approximation, the evolution of chirp parameter $c(z)$ is closely correlated to the random energy and width fluctuations [see Eqs. (19)–(21)]. Obviously, its dynamic behavior is nonlinear, so does the soliton phase evolutions $\phi(z)$ [see Eq. (24)]. As such, in order to solve such nonlinear Langevin equations, we linearize them to analytically solvable forms, only introducing some negligible errors. By virtue of the following change of variables (the subscripts s and 1 denote the deterministic and stochastic terms, respectively)

$$E = E_s + \rho E_1/T_s, \quad T = T_s(1+T_1), \quad c = c_s + \frac{c_1}{2\pi T_s^2},$$

$$\tau_p = \tau_{ps} + \tau_{p1}, \quad b = b_0 + b_1, \quad \text{and} \quad \phi = \phi_s + \phi_1,$$

we transform Eqs. (19)–(24) into their linearized versions,

$$\frac{dE_1}{dz} = \frac{T_s}{\rho}G_E, \tag{31}$$

$$\frac{dT_1}{dz} = -\frac{1}{2}\nu(z)c_1 + \frac{1}{T_s}G_T, \tag{32}$$

$$\frac{dc_1}{dz} = -\nu(z)W_1 + 2\pi T_s^2 G_c, \tag{33}$$

$$\frac{d\tau_{p1}}{dz} = -\beta b_1 + G_{\tau_p}, \tag{34}$$

$$\frac{db_1}{dz} = G_b, \tag{35}$$

$$\frac{d\phi_1}{dz} = -\beta b_0 b_1 + \frac{\pi}{24}\nu(z)(5E_1 + 2T_1) + G_\phi, \tag{36}$$

where $\nu(z)=2\beta/(\pi T_s^2)$, $W_1=E_1-2T_1$, and G_i are the projections of noise on the perturbation functions

$$G_i = \mathrm{Re}\int_{-\infty}^{\infty} g_i^*(z,\tau)\hat{\Gamma}d\tau \quad (i = E,T,c,\tau_p,b,\phi). \tag{37}$$

In terms of Eqs. (31) and (32), we can find easily that

$$\frac{dW_1}{dz} = \nu(z)c_1 + G_W, \tag{38}$$

where $G_W=(T_s/\rho)G_E-(2/T_s)G_T$.

B. Chirp fluctuations

It will be recalled that as a chirped soliton or pulse propagates in a noisy fiber channel, its chirp parameter $c(z)$ will suffer from a random walk [23,26,38]. As such, in order to describe its statistics, we need to solve the coupled Langevin equations (33) and (38). At first sight, for $|\nu(z)| \ll 1$ and within certain distances such that

$$\int_0^z |\nu(z')|dz' \ll 1, \tag{39}$$

the terms proportional to $\nu(z)$ in Eqs. (33) and (38) can be neglected. On this condition, the chirp parameter c_1 is directly driven by the noise source and its probability-density function is exactly Gaussian [40]. Accordingly, integrating Eq. (33) for c_1 and substituting it into $c=c_s+c_1/(2\pi T_s^2)$, we have

$$c(z) = c_s(z) + \frac{1}{T_s^2(z)}\int_0^z T_s^2(z')G_c(z')dz'. \tag{40}$$

As a result, the mean and variance of chirp fluctuations read, respectively, as,

$$\langle c\rangle = c_s(z), \tag{41}$$

$$\sigma_c^2 = \langle c^2\rangle - \langle c\rangle^2 = \frac{2(\pi^2+3)\Gamma_0}{\pi^4 T_s^4(z)}K(z), \tag{42}$$

where $K(z)=-\int_0^z \frac{T_s}{\rho}dz' > 0$. It is clearly seen that the chirp variance is determined by the fiber dispersion and nonlinearity, and does not vanish even for initially chirp-free solitons ($c_0=0$). More interestingly, for an unchirped soliton propagating in optical fibers with constant dispersion and nonlinearity, its chirp variance can grow perfectly linearly with the distance, with its rate of increase inversely proportional to the cube of pulse width. However, all this occurs only for shorter distances determined by the condition (39). This conclusion also can be confirmed by the exact analysis of Eqs. (33) and (38) through the impulse-response function method [23].

By applying the impulse-response method to Eqs. (33) and (38), and carrying out consecutive iterations between c_1 and W_1, one can show that

$$c_1(z_2,z_1) = \cos\left(\int_{z_1}^{z_2}\nu(\zeta)d\zeta\right)\int_{z_-}^{z_+} 2\pi T_s^2(z')G_c(z')dz' - \sin\left(\int_{z_1}^{z_2}\nu(\zeta)d\zeta\right)\int_{z_-}^{z_+} G_W(z')dz', \tag{43}$$

where z_- and z_+ are assumed to be the end points of a short interval centered on z_1, and let it be supposed that there are no perturbations for $z<z_-$. This formula describes the effects

of local noise at z_1 on the chirp evolution at z_2, and is thus referred to as the impulse-response (Green function) equation. Superposing the noise over the whole domain $z_1 \in [0, z_2]$, one can obtain the global formula for $c_1(z_2)$, namely,

$$c_1(z) = \int_0^z \cos[\Theta(z',z)] 2\pi T_s^2(z') G_c(z') dz' - \int_0^z \sin[\Theta(z',z)] G_W(z') dz', \tag{44}$$

where the subscript 2 of distance z has been omitted and

$$\Theta(z',z) = \int_{z'}^z \nu(\zeta) d\zeta = \frac{2}{\pi} \frac{D(z) - D(z')}{T_s(z) T_s(z')}. \tag{45}$$

In the same way, the expression for $W_1(z)$ is found to be

$$W_1(z) = \int_0^z \sin[\Theta(z',z)] 2\pi T_s^2(z') G_c(z') dz' + \int_0^z \cos[\Theta(z',z)] G_W(z') dz'. \tag{46}$$

With these two formulas, both Eqs. (33) and (38) can be verified to be exactly satisfied. Moreover, it is easily seen that only when the condition (39) holds does our exact solution (44), after the same transformation, approach the approximate form (40).

Hence, recalling that $\sigma_c^2(z) = \langle c_1^2(z) \rangle / (4\pi^2 T_s^4)$, and using Eqs. (14), (25)–(27), (37), and (44), one can obtain the exact variance of chirp jitter,

$$\sigma_c^2 = -\frac{2(\pi^2+3)\Gamma_0}{\pi^4 T_s^4(z)} \int_0^z \cos^2[\Theta(z',z)] \frac{T_s(z')}{\rho(z')} dz' - \frac{18\Gamma_0}{5\pi^2 T_s^4(z)} \int_0^z \sin^2[\Theta(z',z)] \frac{T_s(z')}{\rho(z')} dz'. \tag{47}$$

Also, for $|\nu(z)| \ll 1$ and under the condition (39), this exact chirp variance does reduce to the form of Eq. (42). But, for larger distances or otherwise, it would exhibit an oscillating structure as it evolves. This oscillation is not severe and cannot evolve uncontrollably because the value of chirp variance is limited by

$$\frac{2(\pi^2+3)\Gamma_0}{\pi^4 T_s^4(z)} K(z) \le \sigma_c^2 \le \frac{18\Gamma_0}{5\pi^2 T_s^4(z)} K(z). \tag{48}$$

Obviously, such an inequality constraint implies that the trend of increase of chirp variance can still be characterized by the function K/T_s^4, despite small ripples frequently appearing in the growth process.

On the other hand, we notice that, just as mentioned above, the pulse energy and width evolutions come under the influence of chirp fluctuations via fiber dispersion and simultaneously convert such an influence into the phase evolutions [see Eq. (36)], resulting in an extra non-negligible nonlinear phase noise. This appreciable but subtle effect due to chirp fluctuations drew rather little attention in the literature over the years, which maybe stems from the known fact that the Gordon-Mollenauer effect always plays a central role in producing nonlinear phase noise [25]. Indeed, to correctly capture the essentials of phase statistics, chirp fluctuations must be considered. In a subsequent section, we will present an analytical calculation of phase variance and reveal how chirp fluctuations can be converted into nonlinear phase noise.

C. Phase jitter

For this end, we apply the impulse-response method to Eqs. (31), (32), and (35), with results given by

$$E_1(z_2,z_1) = \int_{z_-}^{z_+} \frac{T_s(z')}{\rho(z')} G_E(z') dz', \tag{49}$$

$$T_1(z_2,z_1) = \int_{z_-}^{z_+} \frac{G_T(z')}{T_s(z')} dz' + \frac{1}{2} \int_{z_-}^{z_+} G_W(z') dz' - \frac{1}{2} \sin\left(\int_{z_1}^{z_2} \nu(\zeta) d\zeta \right) \int_{z_-}^{z_+} 2\pi T_s^2(z') G_c(z') dz' - \frac{1}{2} \cos\left(\int_{z_1}^{z_2} \nu(\zeta) d\zeta \right) \int_{z_-}^{z_+} G_W(z') dz', \tag{50}$$

$$b_1(z_2,z_1) = \int_{z_-}^{z_+} G_b(z') dz'. \tag{51}$$

Note that we have used Eq. (43) in the derivation of formula (50). Then, the substitution of Eqs. (49)–(51) into Eq. (36) followed by integrating from z_1 to z_2 yields

$$\phi_1(z_2,z_1) = \int_{z_-}^{z_+} G_\phi(z') dz' - b_0 \int_{z_1}^{z_2} \beta(z') dz' \int_{z_-}^{z_+} G_b(z') dz' + \frac{\pi}{4} \int_{z_1}^{z_2} \nu(z') dz' \int_{z_-}^{z_+} \frac{T_s(z')}{\rho(z')} G_E(z') dz' + \frac{\pi}{24} c_1(z_2,z_1) - \frac{\pi}{24} \int_{z_-}^{z_+} 2\pi T_s^2(z') G_c(z') dz'. \tag{52}$$

This impulse-response equation has simple physical interpretations. The first term on the right-hand side of Eq. (52) represents the direct contribution of ASE noise to phase evolution, which usually is not severe. The phase variations also arise from the frequency fluctuations through dispersion and the energy fluctuations through self-phase modulation, just as indicated by the second and third terms, respectively. Usually, the contributions from them are dominant and the phase noise produced is therefore nonlinear. An intimate inspection of the third term reveals that the net energy fluctuations indeed result from the interplay between energy, width, and chirp fluctuations. In other words, the chirp fluctuations are first converted to the width fluctuations through G_W [see Eq. (50)], then the induced width fluctuations can exactly cancel out the original width fluctuations in phase evolutions, finally resulting in enhanced net energy fluctuations, which, as ex-

plicitly shown in Eq. (52), produce nonlinear phase noise through nonlinearity. As such, we argue that the chirp fluctuations are also an important nonlinear source for producing phase noise, not only their linear effect predicted by the last two terms.

Following the same procedures as used in Eqs. (43)–(47), we obtain the resultant variance of phase jitter,

$$\begin{aligned}\sigma_\phi^2 &= \langle \phi^2 \rangle - \langle \phi \rangle^2 \\ &= \left[\frac{1}{2} + \frac{\pi^2}{6} b_0^2 T_s^2(z) \right] \Gamma_0 K(z) + \left[\frac{2}{3} b_0^2 + \frac{2}{T_s^2(z)} \right] \\ &\quad \times \Gamma_0 \Delta(z) + \left[\frac{\pi^2}{40} S(z) + \frac{\pi^2 + 3}{72} C(z) + \frac{\pi}{3} M(z) \right] \Gamma_0 \\ &= \sigma_{\phi L}^2 + \sigma_{\phi NL}^2 + \sigma_{\phi O}^2, \end{aligned} \tag{53}$$

where $K(z)$ is defined above, and

$$\Delta(z) = -\int_0^z \frac{[D(z) - D(z')]^2}{\rho(z') T_s(z')} dz', \tag{54}$$

$$S(z) = -\int_0^z \sin^2[\Theta(z', z)] \frac{T_s(z')}{\rho(z')} dz', \tag{55}$$

$$C(z) = -\int_0^z \{2 - \cos[\Theta(z', z)]\}^2 \frac{T_s(z')}{\rho(z')} dz', \tag{56}$$

$$M(z) = \int_0^z \frac{D(z) - D(z')}{\rho(z') T_s(z)} \sin[\Theta(z', z)] dz'. \tag{57}$$

We notice that on the right-hand side of Eq. (53), the first, the middle, and the last terms constitute the linear, the nonlinear, and the oscillating parts of the phase variance, which are denoted by $\sigma_{\phi L}^2$, $\sigma_{\phi NL}^2$, and $\sigma_{\phi O}^2$, respectively. Just as mentioned above, the linear and oscillating parts mainly result from the direct noise contribution, the frequency fluctuations, and the chirp fluctuations, including the interplay between them, while the nonlinear one mostly originates in the frequency and energy fluctuations, although the role of chirp fluctuations is likewise essential. Generally speaking, compared to the linear and oscillating parts, the nonlinear one is always dominant, particularly as the pulse duration becomes shorter.

Also, we find from Eqs. (53)–(57) that the phase variance, including each of three parts, can be uniquely determined by the accumulated dispersion $D(z)$ and the ratio of local dispersion to nonlinearity $\rho(z)$ for given noise intensity and initial soliton parameters. The former contributing factor lies at the very heart of the concept of DM and the control of it needs knowledge of both the local profile and the global map of fiber dispersion. By contrast, the contribution of the latter factor is more straightforward, which only affects the phase variance inversely as the magnitude of $\rho(z)$, i.e., the higher the ratio, the smaller the phase variance. In the final analysis, the manipulations of these factors are shown to be full of strategic flexibility, by which the nonlinear phase noise can be significantly reduced (or enlarged) to any desired degree from the point of view of theory. By way of example, the phase variance can be either enlarged or suppressed in the process of pulse broadening, depending on an appropriate choice of fiber parameters and soliton input parameters (see Fig. 3 in the ensuing section).

In addition, the effects of the input soliton parameters such as pulse width τ_0, chirp parameter c_0, and frequency shift b_0 on the control of phase jitter are self-evident as well. We find that although the pulse width of smaller initial value can suppress the linear phase noise to some degree, it may simultaneously increase the nonlinear phase noise drastically and results in an inevitable higher bit-error ratio when communicating. As is the case for τ_0, the initial chirp parameter c_0 manifests itself by the width function $T_s = \tau_0(1 - 2c_0 D)$. Combining Eqs. (53) and (54), we find that the nonlinear phase noise can be significantly reduced if the condition $\mathrm{sgn}(c_0 D) < 0$ is satisfied. As respects the initial frequency shift, we clearly show that it not only causes large timing jitter, an old issue heavily addressed in the past [34,37], but also can produce detrimental nonlinear phase noise, which obviously drew comparatively little attention before. Hence for most practical purposes, the better choice is to eliminate it upon preparation of input solitons.

Certainly, all these findings are interesting and deserve special attention. Hence in the section that follows, we will demonstrate these properties by several numerical evidences and compare them with analytical predictions.

V. NUMERICAL EVIDENCES AND DISCUSSIONS

As far as we know, Eq. (53) is an exact analytical result never reported previously. In terms of this expression, one can evaluate the phase variance analytically for solitons propagating in optical fibers with arbitrary dispersion and nonlinearity without resort to time-consuming numerical simulations. To verify this universal result, we perform numerical simulations of Eq. (13) using the stochastic split-step Fourier code [41] through three intriguing cases. Meanwhile, the properties of phase statistics are also discussed in considerable detail therein. In these simulations, we choose the time step as 0.02 and the spatial mesh as 0.001 with 1000 sample trajectories to reduce both the discretization and sampling errors. The other parameters used in simulations will be specified in the text without confusion. Besides, the numerical evaluation of the phase is implemented according to the phase definition given by Blow *et al.* [42], namely,

$$\phi = \arctan\left[\frac{\int |\psi|^2 \, \mathrm{Im}(\psi) d\tau}{\int |\psi|^2 \, \mathrm{Re}(\psi) d\tau} \right]. \tag{58}$$

A. Constant $\beta(z)$ and $\gamma(z)$

The first demonstration involves the chirp-free system ($c_0 = 0$) with constant dispersion and nonlinearity

$$\beta(z) = \beta_0, \quad \gamma(z) = \gamma_0. \tag{59}$$

This system has been heavily investigated by McKinstrie *et al.* in Ref. [23]. As a special case, it is only mentioned here

to check the consistency between our result (53) and those obtained in Ref. [23]. It follows easily from Eq. (45) that $\Theta(z',z)=\nu_0(z-z')$, where $\nu_0=\nu(0)=2\beta_0/(\pi\tau_0^2)$. In this situation, the functions $K(z)$, $\Delta(z)$, $S(z)$, $C(z)$, and $M(z)$ read, respectively, as

$$K(z)=-\frac{\tau_0\gamma_0}{\beta_0}z, \tag{60}$$

$$\Delta(z)=-\frac{\beta_0\gamma_0}{3\tau_0}z^3, \tag{61}$$

$$S(z)=-\frac{\tau_0\gamma_0}{2\beta_0}\left[z-\frac{\sin(2\nu_0 z)}{2\nu_0}\right], \tag{62}$$

$$C(z)=-\frac{\tau_0\gamma_0}{2\beta_0}\left[9z-8\frac{\sin(\nu_0 z)}{\nu_0}+\frac{\sin(2\nu_0 z)}{2\nu_0}\right], \tag{63}$$

$$M(z)=\frac{\gamma_0}{\nu_0\tau_0}\left[\frac{\sin(\nu_0 z)}{\nu_0}-z\cos(\nu_0 z)\right]. \tag{64}$$

Accordingly, the linear and nonlinear phase noises are provided, respectively, with

$$\sigma_{\phi L}^2=-\left(\frac{1}{2}+\frac{\pi^2 b_0^2\tau_0^2}{6}\right)\frac{\tau_0\gamma_0}{\beta_0}\Gamma_0 z, \tag{65}$$

$$\sigma_{\phi NL}^2=-\beta_0\gamma_0\Gamma_0\left(\frac{2b_0^2}{9\tau_0}+\frac{2}{3\tau_0^3}\right)z^3. \tag{66}$$

We note that the nonlinear contribution, Eq. (66), grows as the cube of the distance and, if discarding the term involving b_0, is completely in agreement with Eq. (73) in Ref. [23]. The oscillating part $\sigma_{\phi O}^2$ is slightly complicated and is exactly determined by Eqs. (62)–(64). It is easily seen that the extrema of $S(z)$ and $M(z)$ lie at $z_{S(M)}=n\pi/\nu_0$, where n is an integer with the same sign as β_0, while $C(z)$ goes to extremes when $z_C=2n\pi/\nu_0$. As such, the oscillating phase variance $\sigma_{\phi O}^2$ is approximately bounded above and below by two straight lines,

$$\mathbb{L}^{+}_{\sigma_{\phi O}^2}=-\frac{58\pi^2+45}{240}\frac{\tau_0\gamma_0}{\beta_0}\Gamma_0 z\simeq-2.57\frac{\tau_0\gamma_0}{\beta_0}\Gamma_0 z, \tag{67}$$

$$\mathbb{L}^{-}_{\sigma_{\phi O}^2}=\frac{22\pi^2-45}{240}\frac{\tau_0\gamma_0}{\beta_0}\Gamma_0 z\simeq 0.72\frac{\tau_0\gamma_0}{\beta_0}\Gamma_0 z. \tag{68}$$

Obviously, in contrast to the nonlinear phase variance, either of the linear and oscillating ones exhibits much less severe (particularly for larger distances) because of their strictly or nearly linear growth. Figure 2(a) depicts the phase variance of an initially unchirped 17.6 ps, measured in terms of the full width at half maximum (FWHM), 0.2 pJ (energy) soliton in a constant dispersion and nonlinearity optical fiber over the propagation of 10 Mm, with analytical results (solid lines) compared to numerical simulations (circles). The effects of frequency shift are considered therein by choosing $b_0=0$ and $b_0=0.1$, respectively (the unit of b_0, THz, has been

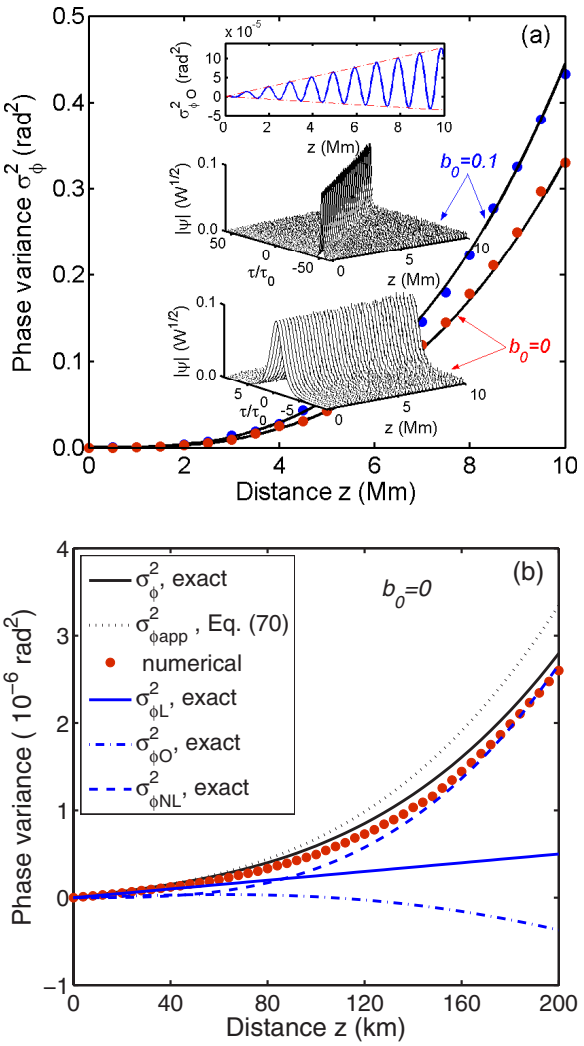

FIG. 2. (Color online) (a) Phase variances of an initially unchirped 17.6 ps (FWHM), 0.2 pJ soliton in an optical fiber with constant dispersion and nonlinearity within the propagation of 10 Mm for different frequency shifts ($b_0=0,0.1$). The solid lines and circles represent the analytical results and the corresponding numerical simulations. Meanwhile, the analytical oscillating phase variance (together with two bounded lines) and the pulse evolutions simulated under different frequency shifts are plotted in the insets as well. (b) Phase variances of the same soliton ($b_0=0$) under identical parametric conditions within 200 km. The dotted line denotes the approximate phase variance given by Eq. (70). The other symbols are the same as described in (a).

omitted for brevity). The typical fiber parameters are given by $\beta_0=-1$ ps^2/km and $\gamma_0=1$ W^{-1}/km. For the sake of comparison, here and in the examples that follow, the intensity of Gaussian white noise is assumed to be $\Gamma_0=5\times10^{-10}$ pJ/km. The top inset shows the oscillating phase variance together with the two bounded lines (67) and (68) versus the propagation distance. The pulse evolutions simulated under different frequency shifts are plotted as well. Notice that the center of the pulse evolution for $b_0=0.1$ has been initially displaced at $\tau_c/\tau_0=50$ for clarity. It is clear that the nonlinear phase noise resulting from frequency and energy (or power) fluctuations dominates over the linear and oscillating contribu-

tions for large distances and the numerical simulations performed are in excellent agreement with our analytical predictions. In particular, we find from the figure along with Eqs. (65) and (66) that the effect of frequency shift on phase noise, either linear or nonlinear, is rather appreciable, particularly for pulse durations larger than 10 ps, unless it is undone at the beginning.

Indeed, for distances far shorter than the dispersion length ($z \ll \tau_0^2/|\beta_0| = L_D$), in other words, when the dispersion effect can be neglected, the oscillating phase variance can be further simplified. On this condition, we can reduce Eqs. (62)–(64) to $S(z)=0$, $C(z)=-(\tau_0\gamma_0/\beta_0)z$, and $M(z)=0$ (the relatively small offsets for them have been omitted). As a result, the oscillating phase noise contribution can be given by

$$\sigma_{\phi O}^2 = -\frac{\pi^2+3}{72}\frac{\tau_0\gamma_0}{\beta_0}\Gamma_0 z \simeq -0.18\frac{\tau_0\gamma_0}{\beta_0}\Gamma_0 z, \tag{69}$$

which also grows linearly, just like the linear phase noise. The phase variance from $\sigma_{\phi L}^2$, $\sigma_{\phi NL}^2$, and $\sigma_{\phi O}^2$ is therefore, if the frequency shift is discarded, equal to

$$\sigma_\phi^2 \simeq -0.68\frac{\tau_0\gamma_0}{\beta_0}\Gamma_0 z - \frac{2\beta_0\gamma_0}{3\tau_0^3}\Gamma_0 z^3. \tag{70}$$

Evidently, compared with Eq. (61) in Ref. [23] which was derived in the absence of dispersion, this result is more suitable because the nonlinear part is exactly correct. We corroborate this result (dotted line) by numerical simulations (circles) in Fig. 2(b) within 200 km under identical parametric conditions. It is easily seen that for distances shorter than 100 km (here $L_D=100$ km) the phase variance can be well approximated by Eq. (70). Apart from this, we also find that the nonlinear phase noise will gain obvious dominance over the linear and oscillating ones as the propagation distance exceeds the dispersion length. Meanwhile, the oscillating phase noise contribution may become negative somewhere because of the counteraction of $M(z)$ on $S(z)$ and $C(z)$ [see Eqs. (55)–(57)]. It should be noted that this phenomenon is indeed not in conflict with the fact that the total phase variance (53) is always positive everywhere during propagation.

B. Exponentially varying $\beta(z)$ and constant $\gamma(z)$

Now we proceed to discuss the system with exponentially varying dispersion and constant nonlinearity [16],

$$\beta(z) = \beta_0 \exp(-\sigma z), \quad \gamma(z) = \gamma_0, \tag{71}$$

where $\beta_0<0$, $\gamma_0>0$, and $\sigma\neq 0$ (note that here σ is just parameter different from the symbolic label σ_ϕ^2 for phase variances in the text). Hence, the fiber gain required for soliton propagation is given by

$$g(z) = -\frac{\sigma(\mu-1)}{\mu-1+\exp(-\sigma z)}, \tag{72}$$

where $\mu=\sigma/(2c_0\beta_0)$. If $\mu=1$, i.e., $c_0=\sigma/(2\beta_0)$, the fiber gain can be completely balanced out and is most gettable in practice. On this condition, the soliton width evolves as $T_s(z)=\tau_0\exp(-\sigma z)$ but the soliton energy remains unchanged, indicating the rapid pulse compression ($\sigma>0$) or pulse broadening ($\sigma<0$) over small distances without radiating dispersive waves [16]. Here without loss of generality, we are concerned with this special but interesting situation.

It follows from Eq. (45) that

$$\Theta(z',z) = \eta(z) - \eta(z'), \tag{73}$$

where $\eta(z)=\nu_0\exp(\sigma z)/\sigma$. Integrating Eqs. (54)–(57) with the above formula, we find, after some algebra, the exact expressions for $K(z)$, $\Delta(z)$, $S(z)$, $C(z)$, and $M(z)$.

$$K(z) = -\frac{\tau_0\gamma_0}{\beta_0}z, \tag{74}$$

$$\Delta(z) = -\frac{\beta_0\gamma_0}{2\tau_0\sigma^3}\{1+2\sigma z-[2-\exp(-\sigma z)]^2\}, \tag{75}$$

$$S(z) = -\frac{\tau_0\gamma_0}{2\beta_0\sigma}\{\sigma z - \sin(2\eta)[\mathrm{Si}(2\eta)-\mathrm{Si}(2\nu_0/\sigma)] - \cos(2\eta) \times[\mathrm{Ci}(2|\eta|)-\mathrm{Ci}(2|\nu_0/\sigma|)]\}, \tag{76}$$

$$C(z) = -\frac{\tau_0\gamma_0}{2\beta_0\sigma}\{9\sigma z - 8\sin(\eta)[\mathrm{Si}(\eta)-\mathrm{Si}(\nu_0/\sigma)] - 8\cos(\eta) \times[\mathrm{Ci}(|\eta|)-\mathrm{Ci}(|\nu_0/\sigma|)] + \sin(2\eta)[\mathrm{Si}(2\eta)-\mathrm{Si}(2\nu_0/\sigma)] + \cos(2\eta)[\mathrm{Ci}(2|\eta|)-\mathrm{Ci}(2|\nu_0/\sigma|)]\}, \tag{77}$$

$$M(z) = \frac{\gamma_0}{\nu_0\tau_0\sigma}\{\eta\sin(\eta)[\mathrm{Ci}(|\eta|)-\mathrm{Ci}(|\nu_0/\sigma|)] - \eta\cos(\eta) \times[\mathrm{Si}(\eta)-\mathrm{Si}(\nu_0/\sigma)] + \cos(\eta-\nu_0/\sigma) - 1\}, \tag{78}$$

where Si and Ci denote the sine and cosine integrals, respectively [43]. Obviously, these final formulas can be applicable for describing the phase statistics of both pulse compression ($\sigma>0$) and pulse broadening ($\sigma<0$).

We begin by discussing the $\sigma<0$ case in which the soliton is continuously broadened. According to Eqs. (53) and (74), the linear part of phase variance reads

$$\sigma_{\phi L}^2 = -\left[\frac{1}{2}+\frac{\pi^2}{6}b_0^2\tau_0^2\exp(-2\sigma z)\right]\frac{\tau_0\gamma_0}{\beta_0}\Gamma_0 z, \tag{79}$$

indicating explicitly that the effect of frequency shift can be greatly amplified as the soliton gets broadened. In this respect, an initial vanishingly small frequency shift would benefit such a soliton broadening. As respects the oscillating part, one can understand its complicated evolution behavior exactly by using Eqs. (76)–(78). But, we also can provide the best estimate of $\sigma_{\phi O}^2$ for large enough distances. Under the circumstances, it is found that $S(z)\simeq 0$, $C(z)=-(\tau_0\gamma_0/\beta_0)z$, and $M(z)\simeq 0$ by using the substitution $\mathrm{Ci}(\xi)\sim -\ln(\Upsilon\xi)$, where $\xi>0$ and Υ is the Euler's constant. Therefore, the oscillating phase variance can be approximately given by

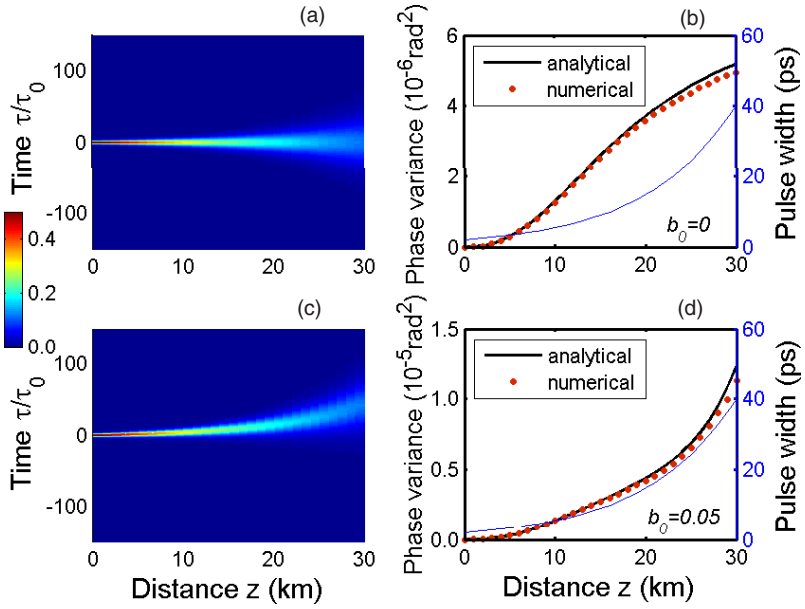

FIG. 3. (Color online) Pulse evolutions and phase variances for an initially chirped soliton ($c_0=5\times10^{-3}$ THz^2) propagating in an optical fiber with exponentially increasing dispersion and constant nonlinearity within 30 km. [(a) and (c)] Pulse evolutions for $b_0=0$ and $b_0=0.05$; [(b) and (d)] the corresponding phase variances (bold lines: analytical; red circles: numerical) together with the changes of pulse width (thin lines). The other parameters have been specified in the text.

$$\sigma_{\phi O}^2 \simeq -\frac{\pi^2+3}{72}\frac{\tau_0\gamma_0}{\beta_0}\Gamma_0 z, \tag{80}$$

which as a rule grows linearly. Also we can obtain the exact nonlinear phase variance as

$$\sigma_{\phi NL}^2 = \left[\frac{2}{3}b_0^2 + \frac{2}{\tau_0^2}\exp(2\sigma z)\right]\Gamma_0\Delta(z), \tag{81}$$

where $\Delta(z)$ is expressed by Eq. (75). It is clear that the second term in square brackets approaches zero (since $\sigma<0$) while with the first term left, which as a result produces exponentially increasing nonlinear phase noise. If the frequency shift is carefully eliminated before soliton injection, the nonlinear phase noise also can be restricted to a vanishingly small level. A close comparison between Eqs. (79) and (81) shows that the linear phase noise in such a system may dominate over the nonlinear one after a propagation of distance, particularly as the initial soliton frequency shift does not vanish.

Taken together, we can conclude from these expressions that the total phase variance would grow linearly in the process of pulse broadening, if the effect of frequency shift is not considered. Figure 3 illustrates these analytical predictions (bold lines) for $b_0=0$ [(a),(b)] and $b_0=0.05$[(c),(d)] under otherwise equal conditions and compares them with numerical simulations (red circles). The left plots demonstrate the pulse evolutions, while the right ones depict their corresponding phase variances and the changes of pulse width (thin lines) versus the propagation distance. Here the initial soliton width and energy are given by $\tau_0=2$ ps and $E_0=1$ pJ. In addition, the fiber parameters used are chosen as $\beta_0=-10$ ps^2/km, $\gamma_0=10$ W^{-1}/km, and $\sigma=-0.1$ km^{-1}, the same as those exploited in Ref. [16]. Correspondingly, the initial chirp parameter is given by $c_0=5\times10^{-3}$ THz^2. It is obvious that the nonlinear phase noise is significantly reduced in Figs. 3(a) and 3(b) but can be drastically amplified (in a nearly exponential scale) in Figs. 3(c) and 3(d), both accompanied by an exponential broadening of pulse width (from 2 ps to nearly 40 ps). Moreover, in either case, numerical simulations are shown to be in good conformity with our analytical results.

However, this is not always the case when solitons suffer from pulse compression in dispersion decreasing fibers ($\sigma>0$). We can find from Eq. (79) that the term involving b_0 would decay rapidly as the soliton gets compressed. Hence, we have $\sigma_{\phi L}^2 \simeq (\Gamma_0/2)K$, irrespective as to whether $b_0=0$ or $b_0\neq0$. In the oscillating part, one can show that the contributions involving $S(z)$ and $C(z)$ are characterized by their central lines, just as discussed in the case of constant dispersion and nonlinearity, but the contribution from $M(z)$ can be characterized by its envelope profile. As a consequence, the oscillating phase variance $\sigma_{\phi O}^2$ is approximately bounded above and below by the following two lines:

$$\mathbb{L}^{\pm}_{\sigma_{\phi O}^2} = -\frac{6\pi^2+15}{80}\frac{\tau_0\gamma_0}{\beta_0}\Gamma_0 z \pm \frac{\pi\gamma_0\Lambda\Gamma_0}{3\tau_0\sigma^2}\exp(\sigma z), \tag{82}$$

where $\Lambda=\{[\pi/2+\mathrm{Si}(\nu_0/\sigma)]^2+\mathrm{Ci}^2(-\nu_0/\sigma)\}^{1/2}$. By contrast with Eqs. (67) and (68), these envelope functions have an exponentially increasing term, which indeed arises from the exponentially decreasing soliton width. Obviously, the more rapidly the pulse width decays, the more severely the value of $\sigma_{\phi O}^2$ oscillates. As respects the nonlinear part, we find that

$$\sigma_{\phi NL}^2 = -\frac{\beta_0\gamma_0\Gamma_0}{\tau_0^3\sigma^3}[(2\sigma z-3)\exp(2\sigma z)+4\exp(\sigma z)-1], \tag{83}$$

in which the comparatively small contribution due to frequency shift has been neglected. Combining the three parts of phase variance into consideration, it is easily concluded that the nonlinear phase noise is still dominant in the process of pulse compression because it nearly grows inversely proportionally to the *square* of pulse width, just as shown in Eq. (53). Figure 4 illustrates these analytical predictions (bold

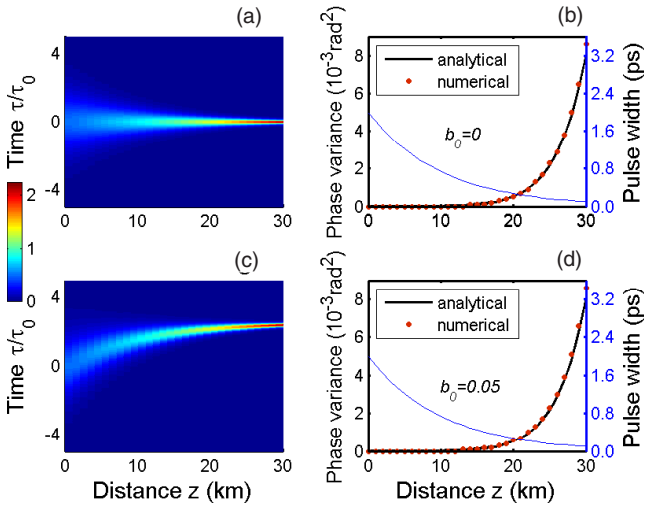

FIG. 4. (Color online) The same as in Fig. 3 except that $c_0=-5\times10^{-3}$ THz^2 and $\sigma>0.1$ km^{-1}, which corresponds to a positively chirped soliton propagating in an optical fiber with exponentially decreasing dispersion and constant $\gamma(z)$.

lines) compared with numerical simulations (red circles) for solitons propagating in a dispersion decreasing optical fiber in which a pulse compression process takes place. As such, we have chosen $\sigma=0.1$ km^{-1} and, correspondingly, $c_0=-5\times10^{-3}$ THz^2 for our present purposes. The other parameters are all the same as those exploited in Fig. 3. Similarly, the left plots [(a), (c)] demonstrate the pulse evolutions under the $b_0=0$ or $b_0=0.05$ case, whereas the right ones [(b), (d)] display the corresponding phase variances together with the changes of pulse width (from 2 ps to nearly 0.1 ps) versus the propagation distance. It is clearly seen that the numerical simulations for both cases coincide very well with our analytical results. Moreover, it is obvious from the figure that an efficient pulse compression is always achieved at the cost of a drastic increase of nonlinear phase noise (e.g., a superexponential growth here). Nonetheless, in contrast to Fig. 3, we show that the effect of frequency shift on phase noise, both linear and nonlinear, is very negligible during such a pulse compression.

C. Cosinoidally varying $\beta(z)$ and $\gamma(z)$

We finally make an approach to an interesting system whose fiber parameters are distributed by [14]

$$\beta(z)=\beta_0\cos(\alpha z),\quad \gamma(z)=\gamma_0\cos(\alpha z), \tag{84}$$

where $\alpha>0$ denotes the frequency of management. It is worth noting that such a cosinoidally managed system will behave like a constant parameter system (59) in the limit $\alpha\to0$, an issue that has been addressed in Sec. V A. Hence, we here are only concerned with the situation that the value of α is comparable to unity. Meanwhile, for the sake of simplicity, the input soliton is assumed to be chirp-free such that one can have an accessible fiber gain $g(z)=0$ in implementation. Under the circumstances, the exact analytical expressions for $K(z)$ and $\Delta(z)$ can be found to be

$$K(z)=-\frac{\tau_0\gamma_0}{\beta_0}z, \tag{85}$$

$$\Delta(z)=-\frac{\beta_0\gamma_0}{\tau_0\alpha^3}\left\{\alpha z\left[\frac{1}{2}+\sin^2(\alpha z)\right]+\frac{3}{4}\sin(2\alpha z)-2\sin(\alpha z)\right\}. \tag{86}$$

It is obvious that the evolution of nonlinear contribution $\Delta(z)$ is mainly ruled by the first term in large brackets and thus exhibits an oscillating increase approximately bounded by two straight lines $\mathbb{L}_\Delta^-$ and $\mathbb{L}_\Delta^+$, namely,

$$\mathbb{L}_\Delta^-=-\frac{\beta_0\gamma_0}{2\tau_0\alpha^2}z,\quad \mathbb{L}_\Delta^+=-\frac{\beta_0\gamma_0}{2\tau_0\alpha^3}(3\alpha z+4). \tag{87}$$

However, one cannot write the resultant analytical expressions for $S(z)$, $C(z)$, and $M(z)$ in terms of elementary functions because the kernel $\sin(\Theta)$ or $\cos(\Theta)$ in Eqs. (55)–(57) cannot be integrated for a composite Θ,

$$\Theta(z',z)=\frac{\nu_0}{\alpha}[\sin(\alpha z)-\sin(\alpha z')]. \tag{88}$$

Therefore, an exact estimate of these functions needs numerical calculations of Eqs. (55)–(57), which can be easily realized by simple algorithms. Numerical analyses show that these oscillating functions, and as a result, $\sigma_{\phi O}^2$, also increase linearly on an average, just like $\Delta(z)$.

The pulse evolutions and the corresponding phase variances for an initially unchirped soliton propagating in such a cosinoidally managed system have been demonstrated in Fig. 5 for two situations: $b_0=0$ and $b_0=0.05$, both with analytical results (bold lines) compared to numerical simulations (red circles). In our simulations, the values of fiber parameters β_0 and γ_0 are the same as those used in Fig. 3 and the frequency of management is chosen as $\alpha=0.2$ km^{-1}. Besides, the input pulse width and energy are given by $\tau_0=2$ ps and $E_0=1$ pJ. Obviously, the numerical simulations performed for both situations are in good agreement with our analytical predictions, and the phase variances are both shown to grow linearly on an average. By comparison, we also note that the contribution of frequency shift to phase noise is not very obvious because here the value of b_0 in Figs. 5(c) and 5(d) is chosen too small, although the pulse evolutions involved are distinguishable. It is only when $|b_0|\sim1/T_s$ holds that the distinction between Figs. 5(b) and 5(d) becomes appreciable, just like the situation shown in Fig. 2(a). This is only a trivial numerical work and is therefore not again provided here for simplicity.

Further, some properties can still be roughly estimated for $S(z)$, $C(z)$, and $M(z)$ if $|\nu_0/\alpha|\ll1$, which corresponds to larger dispersion length and higher frequency of management. This is often the case for picosecond solitons propagating in optical fibers with a relatively small dispersion parameter. As such, up to the first order, one can approximate $\sin(\Theta)$ and $\cos(\Theta)$ to

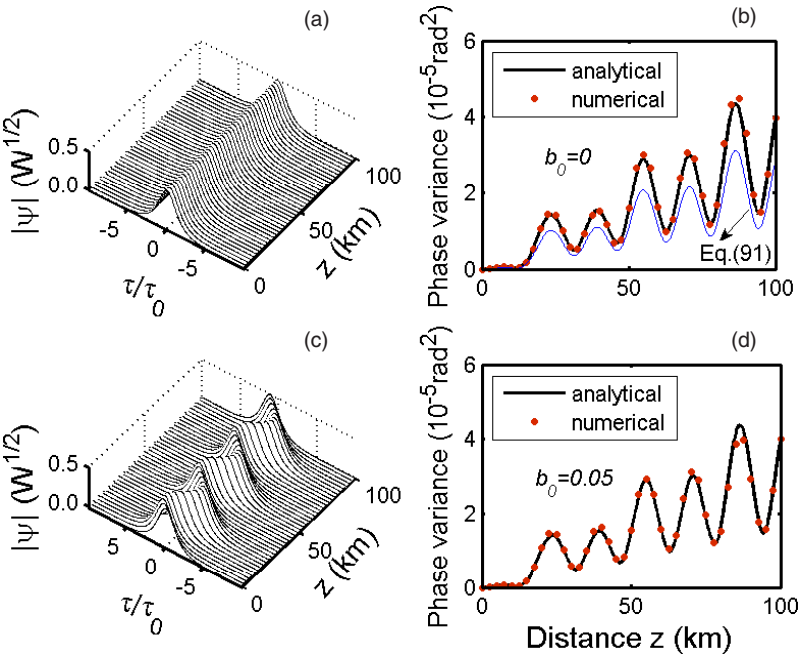

FIG. 5. (Color online) Pulse evolutions and phase variances for an initially unchirped 3.5 ps (FWHM) soliton propagating in a cosinoidally managed optical fiber. [(a) and (b)] b_0=0. [(c) and (d)] b_0=0.05. Bold lines and red circles stand for analytical results and the corresponding numerical simulations. In (b) the approximate phase variance (91) (see text) under existing conditions is also plotted (thin line).

$$\sin(\Theta) \simeq \Theta, \quad \cos(\Theta) \simeq 1. \tag{89}$$

Substituting these into Eqs. (55)–(57) can yield the following rough expressions:

$$S(z) \simeq \frac{4}{\pi^2 \tau_0^2}\Delta(z), \quad C(z) \simeq K(z), \quad M(z) \simeq -\frac{2}{\pi \tau_0^2}\Delta(z), \tag{90}$$

where $K(z)$ and $\Delta(z)$ are given by Eqs. (85) and (86). Accordingly, the phase variance (53) can be simplified as

$$\sigma_\phi^2 \simeq \left(0.68 + \frac{\pi^2}{6} b_0^2 \tau_0^2\right)\Gamma_0 K(z) + \left(\frac{2}{3} b_0^2 + \frac{43}{30\tau_0^2}\right)\Gamma_0 \Delta(z). \tag{91}$$

It is easily concluded from Eqs. (85)–(87) that the phase variance (91) is mainly governed by its first term on the right-hand side and thus grows nearly linearly. The second term involving $\Delta(z)$ usually becomes less important because of $|\nu_0/\alpha| \ll 1$. This implies that in such a cosinoidally managed system the nonlinear phase noise can be significantly suppressed. For comparison, we cite two numerical instances (here setting b_0=0 without loss of generality) in illustration of these rough predictions (see Fig. 6). One is given by the model parameters τ_0=6 ps, β_0=−10 ps^2/km, γ_0 =10 W^{-1}/km, and α=0.2 km^{-1}, which can lead to $|\nu_0/\alpha|$ =0.884; the other corresponds to $|\nu_0/\alpha|$=0.018 by choosing β_0=−1 ps^2/km, γ_0=1 W^{-1}/km, α=1.0 km^{-1}, and an unchanged τ_0. It is clear that only in the latter case does the approximate result (91) (thin crossed line) coincide very well with the analytical result (53) (bold line), which in either case is well consistent with numerical simulations (red circles). The difference between Eqs. (91) and (53) in the former case is mainly caused by the nonlinear phase noise, which becomes more important as the value of $|\nu_0/\alpha|$ increases.

We would like to point out that if the condition precedent under which Eq. (91) is derived is invalidated, in other words, if the frequency α is much less than 1 or the dispersion length becomes smaller, the nonlinear phase noise will become important and may dominate over the linear phase noise. The former statement in our claims is self-evident because as α approaches zero, the nonlinear phase noise will grow as the cube of distance, which we have discussed in Sec. V A. The latter statement also can be confirmed in Figs. 5 and 6 in which the oscillating amplitude arising from the nonlinear phase noise for pulse width equal to 2 ps is more severe than that for the pulse width with 6 ps. However, if the pulse width is of the femtosecond order, we cannot provide our accurate estimate within the framework presented here and one needs to consider an alternative model of Eq.

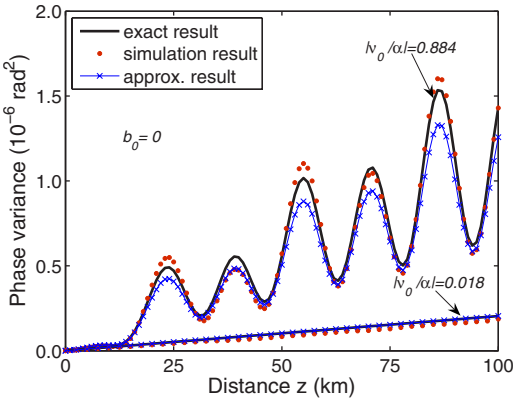

FIG. 6. (Color online) Comparison of phase variances for an initially unchirped 10.6 ps (FWHM) soliton (taking b_0=0) propagating in two cosinoidally varying systems, which correspond to $|\nu_0/\alpha|$=0.884 and 0.018, respectively. The relevant parameters have been specified in the text. Bold lines: exact analytical result (53). Thin crossed lines: approximate result (91). Red circles: numerical simulations.

(13) in which the higher-order dispersive and nonlinear effects must be taken into account [44]. This is an open issue beyond the scope of our present investigation.

VI. CONCLUSIONS

In conclusion, we have reviewed the theoretically and experimentally interesting soliton systems in which the dispersion and nonlinearity can be managed arbitrarily. It is reported that under certain parametric conditions such arbitrarily managed systems would support solitons with a self-similar pulse shape and a strictly linear chirp. The former feature manifests itself by resistance to optical wave breaking and is beneficial to shape-maintained pulse propagation. The latter one, apart from facilitating the subsequent pulse compression via a dispersion delay line, has been shown to make chirped solitons suffer less nonlinear interaction than regular solitons in a collision process. Both of them enable these self-similar soliton pulses to be fascinating information carriers for transoceanic distance transmissions.

In view of the practical relevance to phase-modulated optical communications, we have investigated the phase fluctuations for such sophisticated solitons in a systematical manner. We begin, for practical purposes, by studying the stability problem of these chirped solitons when they are influenced by small perturbations during propagation. Although this issue has been heavily addressed by many numerical works in the past, an analytical exploration is likewise essential. Hence, we present a full linear stability analysis for it and show that an enhanced stability against perturbations is available by virtue of the dispersion management techniques.

We then, by the aid of the variational approach and impulse-response (Green) functions, make an approach to the phase statistics of these solitons, which stems from an inevitable random walk in phase evolutions due to ASE noise. In terms of an unconstrained self-similar soliton ansatz, we present for the first time an exact closed-form expression for the variance of phase jitter in these complicated soliton systems. Notably, in our derivations, the effect of chirp fluctuations has been critically taken into account as well as the dispersive and nonlinear effects. It is found that the chirp fluctuations effect plays an important role in the control of nonlinear phase noise via fiber dispersion, independently of whether the input solitons are initially chirped or not. Significantly, we find from this expression that the phase variance can be uniquely determined by the accumulated dispersion and the ratio of local dispersion to nonlinearity for given noise intensity and some input parameters. This achievement bears on the recent intriguing issues about the control of nonlinear phase noise and may offer effective ways of mitigating the nonlinearity and dispersion penalties.

Last but not least, we corroborate our analytical result (53) with numerical simulations by way of several convincible examples. The first demonstration, as a special case of our universal result, involves the familiar soliton system with constant dispersion and nonlinearity. It not only exactly reproduces some well-known results such as a cubic growth of phase variance with distance and an inverse phase variance dependence on the cube of pulse width, but also renews our view by finding that the residual frequency shift can produce non-negligible nonlinear phase noise apart from causing large timing jitter. We also apply our result to another experimentally accessible soliton system in which the dispersion increases (decreases) exponentially but the nonlinearity remains constant. By choosing appropriate chirp parameter, this special soliton system allows for a rapid pulse broadening (compression) without radiating dispersive waves. We show that the nonlinear phase noise can be greatly suppressed, if the frequency shift effect is eliminated initially, in the process of pulse broadening but drastically amplified as solitons get compressed. We finish our demonstrations with a theoretically intrigued soliton system, which has a cosinoidally varying dispersion and nonlinearity. It is clearly shown that the nonlinear phase noise in such a system can grow linearly on an average, independently of whether the initial frequency shift vanishes or not. Taken altogether, our analytical result can apply to arbitrarily nonlinearity- and dispersion-managed soliton systems within the framework of the generalized NLS equation (13). It is envisioned that our findings may stimulate future experiments and have practical implications for applications in areas such as soliton-based optical communications and optical information processing.

ACKNOWLEDGMENTS

This research was supported in part by the National Natural Science Foundation of China under Grant No. 10574050 and the National Key Basic Research Special Foundation under Grant No. TG1999075206-2. Y.H.Y would like to acknowledge support from the Program for New Century Excellent Talents in University.

[1] N. J. Smith, F. M. Knox, N. J. Doran, K. J. Blow, and I. Bennion, Electron. Lett. **32**, 54 (1996).
[2] B. A. Malomed, *Soliton Management in Periodic Systems* (Springer, New York, 2006).
[3] G. M. Carter, J. M. Jacob, C. R. Menyuk, E. A. Golovchenko, and A. N. Pilipetskii, Opt. Lett. **22**, 513 (1997).
[4] P. V. Mamyshev and L. F. Mollenauer, Opt. Lett. **21**, 396 (1996).
[5] A. Hasegawa, *Massive WDM and TDM Soliton Transmission Systems* (Kluwer, Dordrecht, 2000); L. F. Mollenauer, P. V. Mamyshev, J. Gripp, M. J. Neubelt, N. Mamysheva, L. Grüner-Nielsen, and T. Veng, Opt. Lett. **25**, 704 (2000).
[6] C. Paré, A. Villeneuve, P.-A. Bélanger, and N. J. Doran, Opt. Lett. **21**, 459 (1996); C. Paré, A. Villeneuve, and S. LaRochelle, Opt. Commun. **160**, 130 (1999).
[7] F. Ö. Ilday and F. W. Wise, J. Opt. Soc. Am. B **19**, 470 (2002).
[8] X. Liu, X. Wei, R. E. Slusher, and C. J. McKinstrie, Opt. Lett. **27**, 1616 (2002); C. Xu and X. Liu, *ibid.* **27**, 1619 (2002).

[9] J. D. Ania-Castañón, I. O. Nasieva, S. K. Turitsyn, N. Brochier, and E. Pincemin, Opt. Lett. **30**, 23 (2005).
[10] Q. Quraishi, S. T. Cundiff, B. Ilan, and M. J. Ablowitz, Phys. Rev. Lett. **94**, 243904 (2005).
[11] C. Liberale, V. Degiorgio, M. Marangoni, G. Galzerano, and R. Ramponi, Opt. Lett. **30**, 2448 (2005).
[12] M. Sheik-Bahae, D. C. Hutchings, D. J. Hagan, and E. W. Van Stryland, IEEE J. Quantum Electron. **27**, 1296 (1991).
[13] D. V. Skryabin, F. Biancalana, D. M. Bird, and F. Benabid, Phys. Rev. Lett. **93**, 143907 (2004).
[14] V. N. Serkin and A. Hasegawa, Phys. Rev. Lett. **85**, 4502 (2000); IEEE J. Sel. Top. Quantum Electron. **8**, 418 (2002).
[15] S. K. Turitsyn, T. Schaefer, and V. K. Mezentsev, Phys. Rev. E **58**, R5264 (1998).
[16] V. I. Kruglov, A. C. Peacock, and J. D. Harvey, Phys. Rev. Lett. **90**, 113902 (2003); Phys. Rev. E **71**, 056619 (2005).
[17] S. Chen and L. Yi, Phys. Rev. E **71**, 016606 (2005).
[18] L. Wang, L. Li, Z. Li, G. Zhou, and D. Mihalache, Phys. Rev. E **72**, 036614 (2005).
[19] S. Chen, L. Yi, D.-S. Guo, and P. Lu, Phys. Rev. E **72**, 016622 (2005).
[20] M. E. Fermann, V. I. Kruglov, B. C. Thomsen, J. M. Dudley, and J. D. Harvey, Phys. Rev. Lett. **84**, 6010 (2000); C. Finot and G. Millot, Opt. Express **13**, 7653 (2005).
[21] K.-P. Ho, *Phase-Modulated Optical Communication Systems* (Springer, New York, 2005).
[22] D. Anderson, Phys. Rev. A **27**, 3135 (1983).
[23] C. J. McKinstrie and C. Xie, IEEE J. Sel. Top. Quantum Electron. **8**, 616 (2002).
[24] A. G. Green, P. P. Mitra, and L. G. L. Wegener, Opt. Lett. **28**, 2455 (2003); S. Kumar, *ibid.* **30**, 3278 (2005); K.-P. Ho and H.-C. Wang, *ibid.* **31**, 2109 (2006).
[25] J. P. Gordon and L. F. Mollenauer, Opt. Lett. **15**, 1351 (1990).
[26] T. Hirooka and A. Hasegawa, Opt. Lett. **23**, 768 (1998); J. N. Kutz and P. K. A. Wai, *ibid.* **23**, 1022 (1998).
[27] D. Méchin, S.-H. Im, V. I. Kruglov, and J. D. Harvey, Opt. Lett. **31**, 2106 (2006).
[28] V. N. Serkin, A. Hasegawa, and T. L. Belyaeva, Phys. Rev. Lett. **92**, 199401 (2004).
[29] C. R. Menyuk, D. Levi, and P. Winternitz, Phys. Rev. Lett. **69**, 3048 (1992); S. A. Ponomarenko and G. P. Agrawal, *ibid.* **97**, 013901 (2006).
[30] N. N. Akhmediev and A. Ankiewicz, *Dissipative Solitons* (Springer, New York, 2005).
[31] G. W. Hanson and A. B. Yakovlev, *Operator Theory for Electromagnetics* (Springer, New York, 2002).
[32] D. J. Kaup, Phys. Rev. A **42**, 5689 (1990).
[33] D. E. Pelinovsky, Y. S. Kivshar, and V. V. Afanasjev, Physica D **116**, 121 (1998).
[34] H. A. Haus and W. S. Wong, Rev. Mod. Phys. **68**, 423 (1996). Also see, e.g., the review by R.-J. Essiambre and G. P. Agrawal, in *Progress in Optics*, edited by E. Wolf (North-Holland, Amsterdam, 1997), Vol. 37, p. 185.
[35] S. N. Vlasov, V. A. Petrishev, and V. I. Talanov, Radiophys. Quantum Electron. **14**, 1062 (1971).
[36] M. Hanna, D. Boivin, P.-A. Lacourt, and J.-P. Goedgebuer, J. Opt. Soc. Am. B **21**, 24 (2004); D. Boivin, M. Hanna, P.-A. Lacourt, and J.-P. Goedgebuer, Opt. Lett. **29**, 688 (2004).
[37] E. Iannone, F. Matera, A. Mecozzi, and M. Settembre, *Nonlinear Optical Communications Networks* (Wiley, New York, 1998).
[38] M. V. Kozlov, C. J. McKinstrie, and C. Xie, Opt. Commun. **251**, 194 (2005).
[39] S. Chen, Y. H. Yang, and P. Lu, (to be published).
[40] S. A. Derevyanko, S. K. Turitsyn, and D. A. Yakushev, J. Opt. Soc. Am. B **22**, 743 (2005); C. J. McKinstrie and T. I. Lakoba, Opt. Express **11**, 3628 (2003).
[41] S. Chen, D. Shi, and L. Yi, Phys. Rev. E **69**, 046602 (2004).
[42] K. J. Blow, N. J. Doran, and S. J. D. Phoenix, Opt. Commun. **88**, 137 (1992).
[43] M. Abramowitz and I. A. Stegun, *Handbook of Mathematical Functions* (Dover, New York, 1972).
[44] W. H. Reeves, D. V. Skryabin, F. Biancalana, J. C. Knight, P. St. J. Russell, F. G. Omenetto, A. Efimov, and A. J. Taylor, Nature (London) **424**, 511 (2003); P. D. Drummond and J. F. Corney, J. Opt. Soc. Am. B **18**, 139 (2001).